Structural responses of large-sized floating wind turbine with consideration of mooring-line dynamics based on coupled FEM simulations

Shuangxi Guo, Yilun Li, Min Li, Weimin Chen & Yue Kong

Check for updates

Structural responses of large-sized floating wind turbine with consideration of mooring-line dynamics based on coupled FEM simulations

Shuangxi Guo[a,b,c]*, Yilun Li[d,e]*, Min Li[e], Weimin Chen [a,e] and Yue Kong[d]

[a]Key Laboratory of Mechanics in Fluid Solid Coupling System, Institute of Mechanics, Chinese Academy of Sciences, Beijing, People's Republic of China; [b]AVIC Composite Technology Center, AVIC Manufacturing Technology Institute, Beijing, People's Republic of China; [c]School of Engineering Science, University of Chinese Academy of Sciences, Beijing, People's Republic of China; [d]Université Paris-Saclay, CentraleSupélec, CNRS, MSSMat, Gif-sur-Yvette, France; [e]School of Aeronautics Sciences and Engineering, Beihang University, Beijing, People's Republic of China

ABSTRACT

The dynamic response of a 5 MW floating wind turbine is examined using the coupled finite element simulations, and the dynamic effects of the catenary is considered, while the coupling between flexible components are included. The restoring performance of the mooring-line is analysed based on the vector equations and numerical simulations. The stiffness hysteresis and the influence of the catenary dynamics on the restoring performance are studied. Then the structural responses undergoing wind and wave loads, are examined. Our results show that the mooring-line tension significantly rise due to catenary dynamics, and the snap tension gets around three times larger. The mooring-line stiffness presents a hysteresis character, owing to the fluid/structural damping, which becomes more obvious with the increase of motion frequency/amplitude. Moreover, the structural response gets smaller principally because of the hysteresis effect. The spar displacement and the tower root stress become respectively 18.4% and 32.7% smaller.

1 Introduction

Given the benefits of deep sea wind resources, e.g. steadier wind field, higher wind speed and smaller noise to residents, the wind energy industry is increasingly developed towards deeper ocean area (Wang et al. 2016). More floating wind turbines, including spar, tension-legged, semi-submerged (Rajeswari and Nallayarasu 2020), are considered to operate in ocean area, the floating turbines should be moored through its mooring system to prevent large offset motion from their initial position. Different from the onshore case, the offshore wind turbine suffers environmental loads coming from both the wind and ocean wave/current. Moreover, for a large-sized wind turbine, the dynamic coupling between its flexible parts, such as the blades, tower, and mooring-lines, becomes significant owing to larger structural flexibility and dynamics. Therefore, it's more challenging to analyse the dynamic response of a large-sized floating wind turbine under actions of wind and ocean wave/current (Fazeres-Ferradosa et al. 2020).

The quasi-static method is one of the popular methods originally used in many research studies (Jonkman 2007; Robertson and Jonkman 2011; Karimirad and Moan 2012; Park et al. 2016) about dynamic response, where the restoring force resulting from static displacement is applied on top-end. Or the mooring system is simplified as a non-linear spring, and restoring force is mainly induced by the structural weight of mooring-line. Robertson and Jonkman (2011) used a non-linear spring to model the mooring-line and studied the stability

and external loads of wind turbines with different mooring-line systems. Karimirad et al. (2012) employed an empirical expression of the restoring stiffness based on the experiments. Then the authors built a FEM (finite element method) model of a spar wind turbine and studied its response under environmental loads. Based on the popularly used FAST (Fatigue, Aerodynamics, Structures, and Turbulence) code (Jonkman and Buhl 2007; Browning et al. 2012) where the mooring-line restoring force is calculated through the quasi-static method. Matha et al. (2010) comprehensively studied the natural frequency and response of a TLP (tension leg platform) wind turbine under consideration of the dynamic behaviours. He found that the structural stress may increase, by around 20%, in harsh sea conditions. Using the quasi-static method to model the restoring force of the catenary, Barooni and Ashuri (2018) developed the coupled method of floating wind turbine and programmed the integrated codes to analyse response under wind and wave loads, and Giusti et al. (2017) studied the main influence parameters of dynamic response and the coupling effect between different degrees of freedom of floating platform of wind energy. Actually, in the quasi-static method, the force resulting from the mooring-line motion and its interaction with the ambient fluid are neglected there. That is to say, the structural dynamics, e.g. the inertia and damping effects along with the fluid load acting on the mooring-line are not considered. By applying quasi-static restoring force, Rajeswari and Nallayarasu (2020) investigated the

dynamic response of 3-column and 4-column semi-submersible floaters supporting a wind turbine in regular and random waves.

However, as the mooring-line length increases with the increase of water depth, its dynamic effect becomes more obvious (Waris et al., 2012; Sethuraman and Venugopal 2013). Some research studies (Masciola et al. 2013; Hall and Goupee 2015a; Hall et al. 2015b) indicate that if using quasi-static restoring force, the response of wind turbine may be overestimated. Then the lumped-mass model was developed, where the inertial effect is considered (Palm et al. 2011; Matha et al. 2011). Masciola et al. (2013) studied the impacts of mooring-line inertia and hydrodynamic force on the top tension and rigid body displacement of the semi-submersible wind turbine. He pointed out that the mooring-line dynamics has little effect on the float sway/heave motions, but would induce a significant increase of the top tension; Hall and Goupee (2015a) analysed the tension of the mooring-line under different loads, and he found that quasi-static theory may underestimate the restoring force, and the fatigue load becomes about 30% lower (Hall et al. 2015b). Matha et al. (2011) studied the response of wind turbine with the mooring-line dynamics under consideration and the results showed that the hydrodynamic forces of mooring-line have obvious influence on the body displacement. Kallesoe et al. (2011) pointed out that the load level of structure fatigue may drop, and Azcona et al. (2017) found that the mooring line tension and the tower base loads will significantly change if the dynamic behaviour of the mooring-line is involved. Using a mass-spring model to simulate the mooring lines, Tanaka et al. (2020) studied the dynamic response of a 2-MW spar-type FOWT at the time of typhoon attack in actual sea area.

As the size of floating wind turbines gets larger, the mooring-line dynamics and coupling effect between flexible bodies become more significant. In this study, a fully coupled wind turbine model, which includes flexible blades, tower, floating spar and catenary mooring-lines, is established to consider the impacts of catenary dynamics on global response of a large-sized floating wind turbine. Particularly, the dynamic effect of the catenary mooring-lines and its hysteresis restoring performance are presented. The impacts of mooring-line dynamics on the response of the integrated system under wind and wave conditions are studied. Firstly in Section 2, an approach, including the vector equations of 3D curved flexible beam and the FEM numerical simulation, is developed. Then, the hysteresis character of the restoring stiffness and the influences of the catenary dynamics on its restoring performance are presented in Section 3.1. Finally, the dynamic responses of the integrated system, e.g. the structural displacement and stress of the spar, top tower and the blade, undergoing wind and wave loads, are systematically examined in Section 3.2 and 3.3. Section 4 is our conclusion.

2 The basic equations and FEM numerical simulation models

Previously, two analysis approaches of floating wind turbine, i.e. the multi-body model and multi-degree of freedom model, were used, and the global structures are somewhat simplified into limited degrees of freedom or rigid bodies. To study the response of a spar wind turbine with catenary mooring-lines, the nacelle and rotor were simplified as lumped masses, and then Jeon et al. (2013) examined the change of mooring-line tension with respect to the length and connection position of the mooring-line. Stewart (2012) studied the dynamics of a floating wind turbine atop a tension-leg platform with the modified FAST model. Christiansen et al. (2013a) showed the influence of wind speed and wave frequencies on the platform motion, where the wind load was simplified to horizontal concentration force acting at the tower top. In these research studies, to simplify the wind turbine system during dynamic response analysis, the bodies, such as the blade and tower, are principally regarded as either a lumped-mass or a multi-degree-of-freedom body instead of a flexible body. Here, to include the catenary dynamics, along with the coupling between the flexible bodies of large-sized floating wind turbine, an integrated approach, based on FEM simulations, will be developed.

2.1 Spar type wind turbine

Here the OC3-Hywind spar wind turbine (Jonkman et al. 2009; Jonkman 2010) is taken as the examined example, the NREL 5-MW wind turbine is mounted on a 120 metres draft spar platform moored by catenary mooring-lines, as shown in Figure 1 (a,b). The parameters of the wind turbine system are shown in Table 1.

2.2 Dynamic equations and FEM model of catenary

2.2.1 3D vector expression of a dynamic catenary

Here, the dynamic governing equations, based on the 3D curved flexible beam approach, are applied to consider the non-linear geometry and structural/fluid dynamics of the catenary. In Figure 2, for a 3D catenary, the bottom touching angle φ can be a certain value (in classically static theory, only zero angle was considered). Although the dynamic equations include some non-linear terms that may introduce difficulty in solving dynamic response, they are more reasonable to describing a moving catenary (Sagrilo et al. 2002; Karimirad 2013; Kim et al. 2013; Shin et al. 2013). The governing equations of catenary dynamics can be written by the way of vectors as follows (Chen et al. 2001)

$$\mathbf{T}' + \mathbf{q} = \rho A \ddot{\mathbf{r}} \tag{1}$$

$$\mathbf{Q}' + \mathbf{r}' \times \mathbf{T} + \mathbf{m} = 0 \tag{2}$$

where $\mathbf{r}$ is the position vector of the catenary which depends on the arc length s and time t, as shown in Figure 1. ρ is the catenary mass per unit length and A is the cross-sectional area. $\mathbf{T}$ and $\mathbf{Q}$ are the total force and moment acted on the catenary, respectively, $\mathbf{m}$ are the distributed force and moment. Here, $\mathbf{q}$ includes not only the structural gravity $\rho A g$ but also the hydrodynamic load $\mathbf{f}$, or $\mathbf{q} = \rho A g + \mathbf{f}$, differently from the static case where only the structural gravity $\rho A g$ is included. The hydrodynamic force acting on the

(a) The integrated floating wind turbine under wind&wave loads   (b) The A-A sectional view
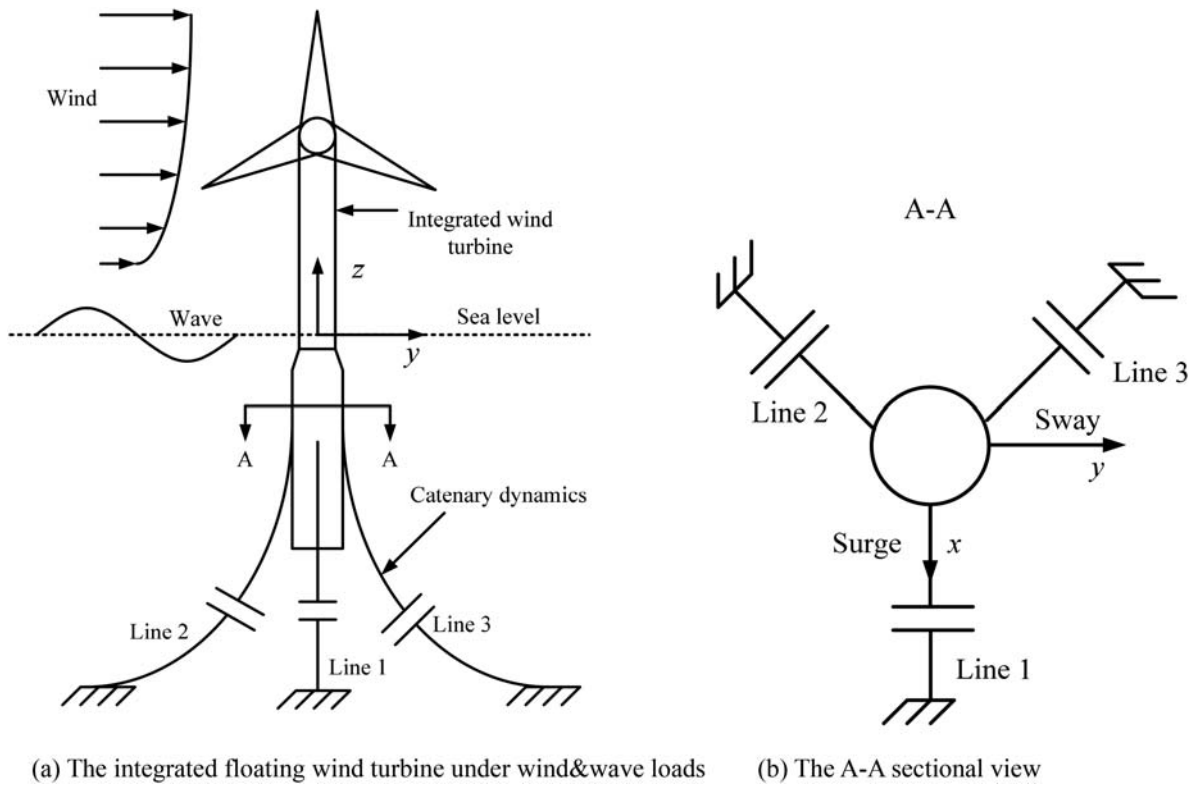
Figure 1. Schematic of the integrated wind turbine system (This figure is available in colour online.).

catenary mooring-line is calculated according to the Morison equation as

$$\mathbf{f} = \frac{1}{2} C_D \rho D |\mathbf{V} - \dot{\mathbf{u}}| (\mathbf{V} - \dot{\mathbf{u}}) + C_A \frac{\pi D^2}{4} \rho (\dot{\mathbf{V}} - \ddot{\mathbf{u}})$$
$$+ \frac{\pi D^2}{4} \rho \dot{\mathbf{V}} \tag{3}$$

where D is the diameter and $\mathbf{u}$ is the displacement of the catenary. $\mathbf{V}$ is the velocity of the amid fluid.

Then the bending moment can be given by the following curvature

$$\mathbf{Q} = \mathbf{r}' \times (EI\mathbf{r}'') + \mathbf{H}\mathbf{r}' \tag{4}$$

where EI is the bending stiffness and $\mathbf{H}$ is the torsion moment. In fact, the rotation moment is small enough, and both $\mathbf{H}$ and $\mathbf{m}$ can be neglected, substituting Equations (4) into (2), we

have:

$$\mathbf{T} = -(EI\mathbf{r}'')' + \lambda \mathbf{r}' \tag{5}$$

Substituting Equation (5) into (1) yields

$$-(EI\mathbf{r}'')'' + (\lambda \mathbf{r}')' + \mathbf{q} = \rho A \ddot{\mathbf{r}} \tag{6}$$

The equation of strain is

$$\mathbf{r}' \cdot \mathbf{r}' = (1 + \varepsilon)^2 \tag{7}$$

where $\varepsilon = T_L/EA$ is the catenary strain, and $\mathbf{T}_L$ is the location tension of the catenary. If the value of the bending moment in Eq.(6) is zero, we will have the governing equation of a flexible catenary of which the loads include not only the static structural gravity but also the dynamic fluid load as follows:

$$(\lambda \mathbf{r}')' + \mathbf{q} = \rho A \ddot{\mathbf{r}} \tag{8}$$

Combing Equations (7) and (6) or (8), we have the non-linear

Table 1. Main parameters of the wind turbine system.

| Parameters	Value	Parameters	Value
Tower height above water	87.6 m	Mooring-line length	800.0 m
Material density of tower	8500.0 kg/m³	Rotor diameter	126.0 m
Depth to spar base below water	120.0 m	Blade length	61.5 m
Spar total mass	7466330.0 kg	Hub diameter	3.0 m
Equivalent mooring-line weight in water	698.1 N/m	Rated wind speed	11.4 m/s
Depth to anchors below water	420.0 m	Blade mass	17740.0 kg
Horizontal projection mooring system	706.0 m		
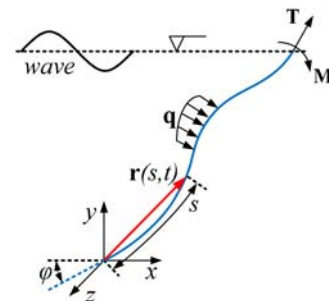
Figure 2. The schematic diagram of a dynamic catenary (This figure is available in colour online.).

governing equations of the dynamic catenary. Since the governing equations could not be directly solved, they will be numerically solved by employing finite element simulations.

2.2.2 FEM model of dynamic catenary

Two-node Euler beam element is used as the basic element of the catenary, which is able to provide tension stiffness and also available to bear transverse force caused by ambient fluid during dynamic response. The catenary is uniformly divided so that the laterally distributed load of the ambient fluid, consisting of the hydrodynamic inertia and drag terms, can be conveniently acted on the beam elements. For representativeness and simplicity, we consider only three DOFs (degrees of freedom), i.e. two translation displacements in x-y plane, u_i and v_i ($i = 1, 2, \ldots, N+1$), plus one rotation angle around z axis, θ_i, of per node. The dynamic equation of the catenary can be written as follows:

$$(\mathbf{M}_C + \bar{\mathbf{M}}_C)\ddot{\mathbf{U}}_C + \mathbf{C}_C\dot{\mathbf{U}}_C + \mathbf{K}_C\mathbf{U}_C = \mathbf{F}_C \tag{9}$$

where $\mathbf{M}_C$ is the mass matrix and $\bar{\mathbf{M}}_C$ is the added mass matrix. $\mathbf{C}_C$ is the structure damping matrix. $\mathbf{K}_C$ is the stiffness matrix. $\mathbf{U}_C$ and $\mathbf{F}_C$ are, respectively, the displacement and external force vectors. Owing to the large flexibility of the moving catenary, the value of its rotation and translation displacement may be large too. To model this situation, the constrain of rotational DOFs of two connecting beam element is not included in our numerical simulation. Subsequently, due to this additional rotation DOF of connection grid, the displacement vector of each catenary element will have more DOFs (Guo et al. 2017) as follows.

$$\mathbf{U}_{Ci} = [u_i, v_i, w_i, \theta_i, u_{i+1}, v_{i+1}, w_{i+1}, \theta_{i+1}]^T \quad i = 1, N$$
$$\mathbf{U}'_{Ci} = [u_i, v_i, w_i, \theta_i, \theta'_i, u_{i+1}, v_{i+1}, w_{i+1}, \theta_{i+1}, \theta'_{i+1}]^T \quad i = 2, \cdots, N-1 \tag{10}$$

Comparing Equation (11) with the previous one, i.e.

$$\mathbf{U}_{Ci} = [u_i, v_i, w_i, \theta_i, u_{i+1}, v_{i+1}, w_{i+1}, \theta_{i+1}]^T$$
$$i = 1, N \tag{11}$$

it is seen that there are two additional DOFs, i.e. θ'_i and θ'_{i+1}, which could introduce in-determinacy of the governing equations. In that case, additional constrains are required to solve out the dynamic responses. Here, the special initial condition, i.e. a pre-stressed top tension calculated according to the static method along with the statically equilibrium configuration, is employed to meet the deterministic condition of the solution. More specifically, under the original static shape and still status, the catenary is balanced according to statics, or the structural tensions and gravity can keep the catenary body statically determined. And, the two adjacent beams have the same angle at the connection nodes. If the catenary dynamically moves under the wave load, the system is governed by both static and dynamic terms, as shown in Equations (1) and (2). Then the additional dynamics can carry on the additional rational DOF, and we can get the dynamic response of the catenary.

2.3 Coupled FEM model of integrated wind turbines

Regarding the slender bodies, i.e. the blades' tower and spar, every single body is divided into several beam elements. Regarding the body forces, e.g. the centrifugal force coming from the blade rotation and structural gravity of large-sized bodies, the axial DOF of the beam element is also included. The beam element is shown in Figure 3, and its displacement vector is

$$\mathbf{U}_e = [u_{1j}, u_{2j}, u_{3j}, \theta_{1j}, \theta_{2j}, \theta_{3j}, u_{1j+1}, u_{2j+1}, u_{3j+1}, \theta_{1j+1}, \theta_{2j+1}, \theta_{3j+1}] \tag{12}$$

where the direction 1 is along the beam axle, and directions 2 and 3 are lateral. j is the node number. For simplicity of representativeness, the displacement vector can be rewritten as involving two parts, i.e. the axial and lateral parts, as follows.

$$\mathbf{U}_e^1 = [u_{1j}, u_{1j+1}], \mathbf{U}_e^2 = [u_{2j}, \theta_{3j}, u_{2j+1}, \theta_{3j+1}] \text{ and } \mathbf{U}_e^3 = [u_{3j}, \theta_{2j}, u_{3j+1}, \theta_{2j+1}] \tag{13}$$

Then the stiffness matrices corresponding to respectively the axial and lateral displacements are

$$\mathbf{K}_e^1 = \int_0^{l_e} \int_{A_e} \mathbf{B}_1^T E_e \mathbf{B}_1 dA_e dx_e \qquad \mathbf{M}_e^1 = \int_0^{l_e} \int_{A_e} \mathbf{N}_1^T \rho_e \mathbf{N}_1 dA_e dx_e$$
$$\mathbf{K}_e^{2,3} = \int_0^{l_e} \int_{A_e} \mathbf{B}_{2,3}^T E_e \mathbf{B}_{2,3} dA_e dx_e \quad \mathbf{M}_e^{2,3} = \int_0^{l_e} \int_{A_e} \mathbf{N}_{2,3}^T \rho_e \mathbf{N}_{2,3} dA_e dx_e \tag{14}$$

where l_e, x_e and A_e are the beam element length, axial location and cross section area, respectively. The strain matrix $\mathbf{B}_i(x) = d\mathbf{N}_i(x_e)/dx_e$. The displacement functions are

$$\mathbf{N}_1(x_e) = [1 - x_e/l_e, x_e/l_e] \, \mathbf{N}_{2,3}(x_e) = [1 - 3\xi^2 + 2\xi^3, l_e(\xi - 2\xi^2 + \xi^3), 3\xi^2 - 2\xi^3, l_e(\xi^3 - \xi^2)]$$

where $\xi = x_e/l_e$. Based on the above element matrices, i.e. the stiffness matrix $\mathbf{K}_e$ and mass matrix $\mathbf{M}_e$ in Eq. (14), the whole structural matrices can be obtained through the transfer matrix $\mathbf{T}_n$ as follows

$$\mathbf{K} = \sum_{N_{sys}} \mathbf{T}_e^T \mathbf{K}_e \mathbf{T}_e \quad \mathbf{M} = \sum_{N_{sys}} \mathbf{T}_e^T \mathbf{M}_e \mathbf{T}_e \tag{15}$$

where

$$\mathbf{T}_n = \begin{bmatrix} [\mathbf{0}] & \cdots & \overset{j}{[\mathbf{I}]} & \cdots & \overset{k}{[\mathbf{I}]} & \cdots & [\mathbf{0}] \end{bmatrix} \tag{16}$$
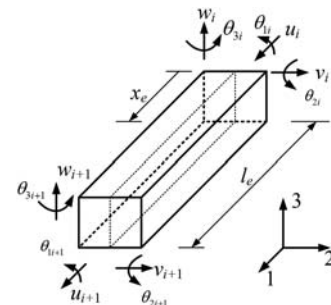

Figure 3. The beam element in the local coordinate system (This figure is available in colour online.).

Here $[\mathbf{I}]$ is a unit matric with 12 dimensions (6 DOFs per node times 2 nodes of every single beam element), and $\mathbf{T_n}$ is $12 \times N_{sys}$ where N_{sys} is the number of the system's DOFs.

Actually, the DOFs of the integrated system consist of three components, i.e. the displacement vector U_B including the blade and nacelle displacements, the displacement vector U_S including the spar and tower displacements, and U_M is the displacement of the mooring system. Now, the coupled equations of the integrated system can be written as follows:

$$
\begin{bmatrix} \mathbf{M}_{BB} & \mathbf{M}_{BS} & \mathbf{0} \\ \mathbf{M}_{SB} & \mathbf{M}_{SS} & \mathbf{M}_{SM} \\ \mathbf{0} & \mathbf{M}_{MS} & \mathbf{M}_{MM} \end{bmatrix} \begin{bmatrix} \ddot{\mathbf{U}}_B \\ \ddot{\mathbf{U}}_S \\ \ddot{\mathbf{U}}_M \end{bmatrix}
$$
$$
+ \begin{bmatrix} \mathbf{C}_{BB} & \mathbf{C}_{BS} & \mathbf{0} \\ \mathbf{C}_{SB} & \mathbf{C}_{SS} & \mathbf{C}_{SM} \\ \mathbf{0} & \mathbf{C}_{MS} & \mathbf{C}_{MM} \end{bmatrix} \begin{bmatrix} \dot{\mathbf{U}}_B \\ \dot{\mathbf{U}}_S \\ \dot{\mathbf{U}}_M \end{bmatrix}
$$
$$
+ \begin{bmatrix} \mathbf{K}_{BB} & \mathbf{K}_{BS} & \mathbf{0} \\ \mathbf{K}_{SB} & \mathbf{K}_{SS} & \mathbf{K}_{SM} \\ \mathbf{0} & \mathbf{K}_{MS} & \mathbf{K}_{MM} \end{bmatrix} \begin{bmatrix} \mathbf{U}_B \\ \mathbf{U}_S \\ \mathbf{U}_M \end{bmatrix}
$$
$$
= \begin{bmatrix} \mathbf{F}_B \\ \mathbf{F}_S \\ \mathbf{F}_M \end{bmatrix} \tag{17}
$$

where $\mathbf{M}_{ij}$, $\mathbf{C}_{ij}$ and $\mathbf{K}_{ij}$ ($i, j = B, S, M$) are, respectively the mass matrix, damping matrix and stiffness matrix of different components. It is worth noting that the non-diagonal terms of the matrices actually indicate the non-linear dynamic coupling between the wind turbine components, which were mostly neglected if the uncoupled approach is used.

It is also noted that, on the boundary of two adjacent components, the boundary nodes, e.g. connecting blade root and tower top, essentially belong to both components, which actually have at the same position. So the displacement vectors $\mathbf{U}_B$ and $\mathbf{U}_S$ have the same DOFs of the boundary node, and it is required to use the coincident node. In other words, similarly with the process of assembling elements as a whole structure, the value of the corresponding item in the assembling matrix is the sum of the two components. In order to avoid matrix singularity in response calculation, the multipoint constraints are used to connect the bodies with large difference of the stiffness value in the developed FEM model.

At last, super-element is used for the mooring-line part for better efficiency of computation process. Given the non-linearity of the catenary, the values of the beam element length and the time step during dynamic response should be small enough to obtain an acceptable numerical accuracy. On the other hand, this may introduce an expensive computation cost in terms of calculation time and computer resources. Therefore, super-element is used for every single catenary of the mooring system.

Generally speaking, each catenary is processed independently resulting in a set of matrices that are reduced to a boundary and describe the behaviour of the catenary, as seen by the rest of the wind turbine. The reduced boundary matrices for the individual super-elements are combined to form the assembly matrices which are referred to as the residual matrices. The residual matrices are solved for calculating displacements. The residual solution is then imposed on the boundary of each super-element so that the data recovery for the boundary can be combined with the data recovery for the body loads on the super-element. For example, the stiffness matrix of a catenary can be rewritten as

$$
\begin{bmatrix} \mathbf{K}_{bb} & \mathbf{K}_{bo} \\ \mathbf{K}_{ob} & \mathbf{K}_{oo} \end{bmatrix} \begin{bmatrix} \mathbf{U}_b \\ \mathbf{U}_o \end{bmatrix} = \begin{bmatrix} \mathbf{P}_b \\ \mathbf{P}_o \end{bmatrix} \tag{18}
$$

where $\mathbf{U}_b$ and $\mathbf{U}_o$ are, respectively, the boundary and interior displacements. Then the reduced matrix equation is

$$
\begin{bmatrix} \mathbf{K}_{bb}^* & \mathbf{0} \\ \mathbf{K}_{ob}^* & \mathbf{I} \end{bmatrix} \begin{bmatrix} \mathbf{U}_b \\ \mathbf{U}_o \end{bmatrix} = \begin{bmatrix} \mathbf{P}_b^* \\ \mathbf{P}_o^* \end{bmatrix} \tag{19}
$$

where

$$
\mathbf{K}_{bb}^* = \mathbf{K}_{bb} - \mathbf{K}_{bo}\mathbf{K}_{oo}^{-1}\mathbf{K}_{ob}, \quad \mathbf{P}_b^* = \mathbf{P}_b - \mathbf{K}_{bo}\mathbf{K}_{oo}^{-1}\mathbf{P}_o
$$
$$
\mathbf{K}_{ob}^* = \mathbf{K}_{oo}^{-1}\mathbf{K}_{ob}, \quad\quad\quad \mathbf{P}_o^* = \mathbf{K}_{oo}^{-1}\mathbf{P}_o \tag{20}
$$

It should be pointed out that the process from Equations (18)–(19) is done by using the Gaussian-Jordan elimination method rather than a matrix manipulation. Data recovery for each super-element is performed by expanding the solution at the attachment points, using the same transformation that was used to perform the original reduction on the super-element. As we get the boundary displacement vector $\mathbf{U}_b$, we can obtain the displacement vector of the interior nodes by the second formula of Equation (19) as

$$
\mathbf{U}_o = \mathbf{P}_o^* - \mathbf{K}_{ob}^*\mathbf{U}_b \tag{21}
$$

The right side term of Equation (17) is the load term which can be categorised into the three parts, the first part $\mathbf{F}_B$ is the force acting on the blades and tower, which includes the wind force and centrifugal force induced by the rotating blade. The second part $\mathbf{F}_S$ is the load acting on the spar mainly coming from the ocean wave. The third part $\mathbf{F}_M$ includes the hydrodynamic force acting on the mooring-line. The gravity force is also included in all the three parts. Here, all the loads, i.e. the wind and wave force, the inertia and damping force and dynamic restoring force of the mooring system are included in the dynamic equation of the wind turbine system. To solve the non-linear equation, the Newmark method is used.

2.4 The random wind and wave loads

The random wind and wave loads are considered here, in order to generate the time history of the random wind, the mostly used Kaimal spectrum (Hansen 2013) is chosen here to calculate the time history approximation of wind speed and the consequent wind load. The wind speed spectrum is

$$
PSD(f) = \frac{I^2 V_{10\,\text{min}} l}{(1 + 1.5\dfrac{fl}{V_{10\,\text{min}}})^{5/3}} \tag{22}
$$

where I is the turbulence intensity. $V_{10\,\text{min}}$ is the average wind speed in ten minutes at the given point. l is the scalar taking value. It is assumed that the wind load uniformly acts on every blade, and the value of wind speed is the same with that at the hub height. For simplicity, an approximate wind thrust force is computed for the complete swept area of the

blades following the method of Christiansen et al. (2013b)

$$F_{\text{thrust}} = \frac{1}{2} C_T \rho_{\text{air}} A_b V_{rel}^2 \tag{23}$$

where ρ_{air} is the density of air, and A_b is the swept area of the blades. C_T is the thrust coefficient, and V_{rel} is the amplitude of the velocity of the wind relative to that hub.

As for the random wave loads, we use the JONSWAP spectrum (Li et al. 2018), an empirical relationship that defines the distribution of the wave energy, to generate the time history of the ocean wave speed. The equation of the JONSWAP spectrum is

$$S(\omega) = \frac{\alpha g^2}{\omega^5} \exp\left[-\beta \frac{\omega_p^4}{\omega^4}\right] \gamma^a \tag{24}$$

where

$$a = \exp\left[-\frac{(\omega - \omega_p)^2}{2\omega_p^2 \sigma^2}\right] \quad \sigma = \begin{cases} 0.07 & \omega \le \omega_p \\ 0.09 & \omega \ge \omega_p \end{cases} \quad \beta = 1.25$$

And α is a constant, ω is the wave frequency and ω_p is the peak wave frequency, g is the gravity acceleration. Using Equation (24) we can obtain the time history of the random wave, then the wave force acting on the spar can be derived. As the spar is a slender cylindrical structure, where the diffraction regime is not that significant for the calculation of the wave loads, the Morison equation is applied to obtain the hydrodynamic force, and here the added mass and damping coefficients for the spar are 0.97 and 0.6, respectively (Jonkman 2010).

2.5 Verification of the FEM models and dynamic characteristics of the integrated wind turbine

As we know, to examine the dynamic response and stability of a floating system, six rigid body motions are usually considered. For this spar wind turbine, its motion performance in surge and sway direction is determined by the restoring force of the mooring system, while its heave and pitch motions mainly depend on the inertia property of spar itself. Given the well-designed stability of its heave motion, only the surge and pitch responses of the spar are presented in this study to evaluate the performance of the wind turbine system. A multiflexible-body FEM model of the integrated wind turbine including several parts, i.e. the blades, nacelle, tower, spar

and mooring systems, was developed, and the FEM model is shown in Figure 4(a–c).

To model the elasticity of the flexible bodies, each blade is divided into 123 beam elements, and the tower is divided into 100 beam elements. As for the catenary mooring-line, special beam elements, of which the rotation degree is released between neighbouring ends, are used, and the bending stiffness of special beam element is ignored. Every single mooring-line is divided into 400 elements. The Morison equation is used to obtain the hydrodynamic force of the ambient fluid acting on the mooring-line, in which the drag coefficient is 1.2 (Jonkman 2010).

2.5.1 Comparison of the dynamic mooring-line model with the experiment

To verify our dynamic mooring-line model, the top tensions and displacements of a catenary under top-end surge and heave motions are calculated and compared to the experiment (Barrera et al. 2019). The schematic of the catenary is shown in Figure 5(a), and its main parameters are given in Table 2 (Barrera et al. 2019). Here three cases are considered, i.e. in surge case, the top-end is moving amplitude is 75 mm with 1.58s and 3.16s period. In heave case, the top-end moves with heave 75 mm amplitude and 2.21s period.

The top tension and displacement are compared to the experiments in Figure 5. Figure 5(b,c) show that there is an acceptable agreement with the numerical and experimental results, though the time history of top tension has a certain phase difference. For the surge case, the predicted minimum tension is almost the same with the experiment, and the difference of the maximum tension is about 5.1%, i.e. 8.73N of calculated value compared to 8.29N of experiment. For heave case, as shown in Figure 5(c), the numerical top tension is slightly higher, by about 3%, than the experimental value, both the maximum and minimum values. The value comparisons of the catenary tensions are listed in Table 3, the differences between numerical and experimental results can be estimated by the following equation

$$Es = \frac{T_{\text{num}} - T_{\text{exp}}}{T_{\text{exp}}} \times 100\% \tag{25}$$

where E_s represents the difference, T_{num} is the calculated tension and T_{exp} is the experimentally measured tension. It can be seen that the differences are less than 5.1%, or our numerical model can give good prediction of dynamic catenary response.
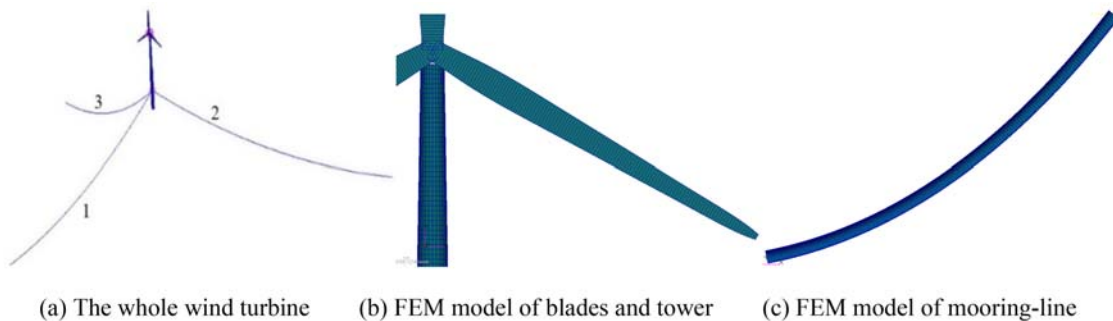

(a) The whole wind turbine   (b) FEM model of blades and tower   (c) FEM model of mooring-line

Figure 4. FEM model of the integrated wind turbine system (This figure is available in colour online.).

(a) Schematic of the experimental catenary

(b) Top tension under top-end surge motion

(c) Top tension under top-end heave motion

(d) Vertical displacement of marker 1

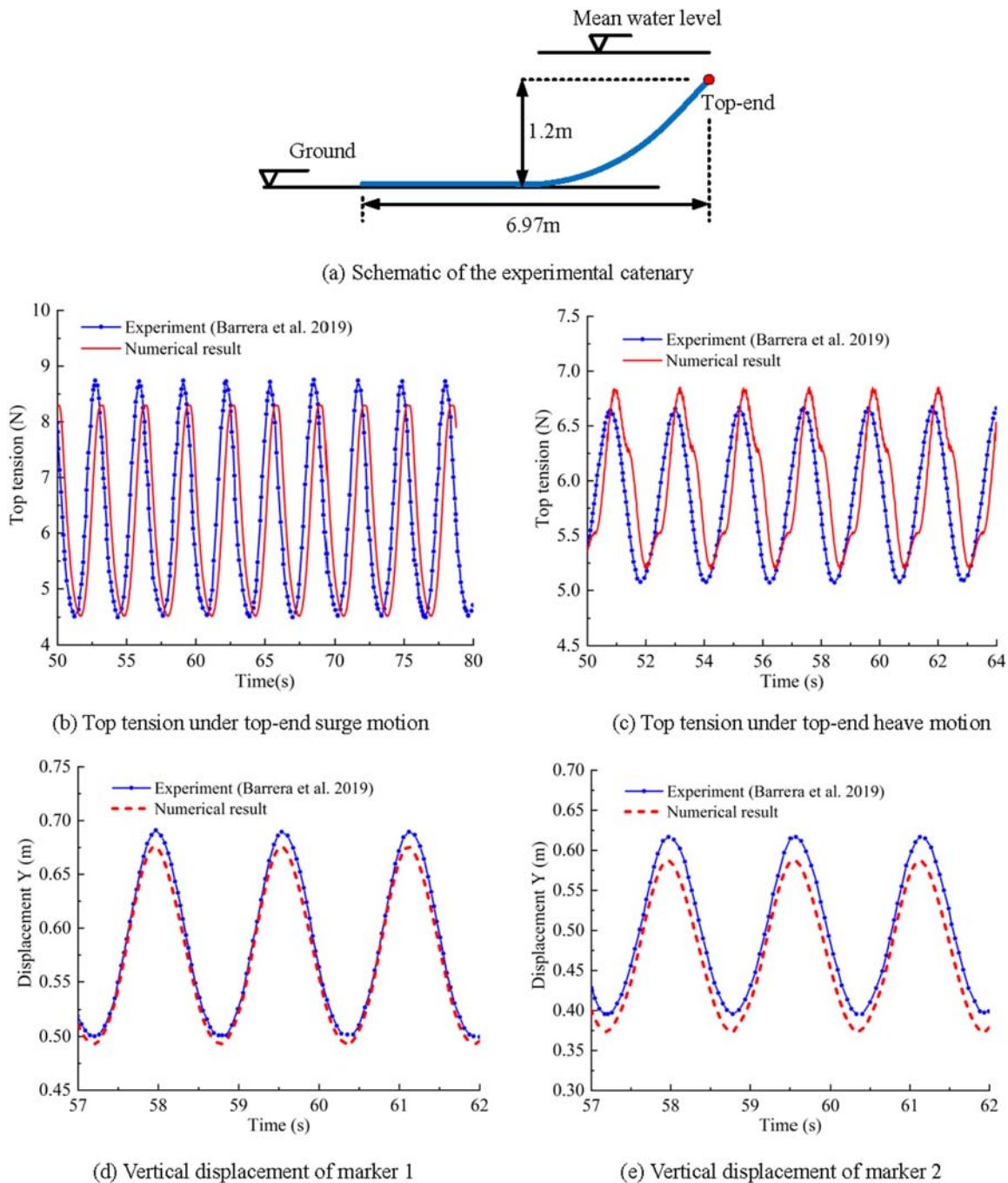(e) Vertical displacement of marker 2

Figure 5. Schematic of the catenary and response comparisons (This figure is available in colour online.).

The vertical displacements of the two markers, i.e. respectively located at 1.0 m (Marker 1) and 1.2 m (Marker 2) from the top-end point (Carlos et al, 2019), are shown in Figure 5(d, e). It can be seen that the numerical results agree well with the experimental one, e.g. the difference is less than 4.9% (0.586 m of calculated value compared to 0.616 m of experiment).

2.5.2 Global dynamic characteristics of integrated wind turbine

Based on the developed coupled FEM model of the integrated floating wind turbine, the global dynamic characteristics along with response could be given. Here the dynamic characteristics of the integrated system are

Table 2. Parameters of the catenary.

Parameter	Value	Parameter	Value
Total length	7.305 m	Mass in air	0.162 kg/m
Initial horizontal projection	6.97 m	Equivalent diameter	0.0052 m
Initial vertical projection	1.2 m	Elastic modulus	77.2 GPa

Table 3. Comparison of the catenary tension.

Cases	Tension	Numerical/N	Experimental/N	Error/%
Surge	Maximum	8.29	8.73	5.1
	Minimum	4.52	4.51	0.2
Heave	Maximum	6.85	6.66	2.8
	Minimum	5.23	5.08	2.9

Table 4. Natural frequencies of the wind turbine Unit: rad/s

Wind Turbine Modes	Predicted Value	(Karimirad 2013)	Difference /%
Surge	0.0524	0.05	4.46
Sway	0.0524	0.05	4.46
Pitch	0.224	0.221	1.75
Roll	0.227	0.221	2.81
Mooring-lines first bending	0.3707	/	/
Mooring-lines second bending	0.7036	/	/
Mooring-lines third bending	1.0686	/	/
Tower first bending	2.7558	/	/
Blade first bending	4.5863	/	/

calculated, and they are compared with the published result (Karimirad 2013) to verify our FEM model, see Table 4 and Figure 6. Table 4 gives the period comparison of our results to the other (Karimirad 2013), it can be seen that the predicted value agrees well with the published one, and the difference is less than 5%.

Figure 6 shows that, in addition to the rigid-body modes [see Figure 6(a,b)], the coupled FEM model is able to give more elastic modes, such as Figure 6(c,d). It is noted that the periods of certain modes of the integrated wind turbine, e.g. the first three bending modes of the mooring-line and the first bending mode of the blade or tower, fall in the range of the wave periods. That may introduce a larger-amplitude response at higher frequencies, which could influence the structure fatigue life and should be paid attention during dynamic response analysis.

3. Non-linear restoring performance of mooring-line and structural response of the wind turbine

The regular wave (Shin et al. 2013) and the random wind together with the irregular wave (Karimirad 2013; Cheng et al. 2017) load cases are summarised in Table 5. Here, the initial condition is that all bodies are still originally. To examine the impact of catenary dynamics on the structural response, the response of the integrated system with quasi-static restoring force is also calculated.

3.1. Restoring performance of the catenary with its dynamic effects under consideration

The dynamic tension and the non-linear restoring stiffness will be discussed, and compared with the quasi-static cases, to examine the impacts of the catenary dynamics.

3.1.1 The dynamic restoring tension

The top tension response of Line 1 in time domain (see Figure 1 (b)) is presented in Figure 7. It is seen that the dynamic tension is slightly larger than the quasi-static one, and the difference is not obvious if the surge amplitude/frequency is smaller, e.g. 2 m amplitude and 20s period, as shown in Figure 7(a). But the dynamic tension gets larger than the quasi-static value with the increase of the amplitude/frequency of the top-end motion. For example, at 3 m amplitude and 10s period in Figure 7(b), the tension amplitude is 1.5 times larger than the quasi-static value.

Moreover, the tension gap (between peak and trough) gets 4 times larger than the quasi-static value. That increase of
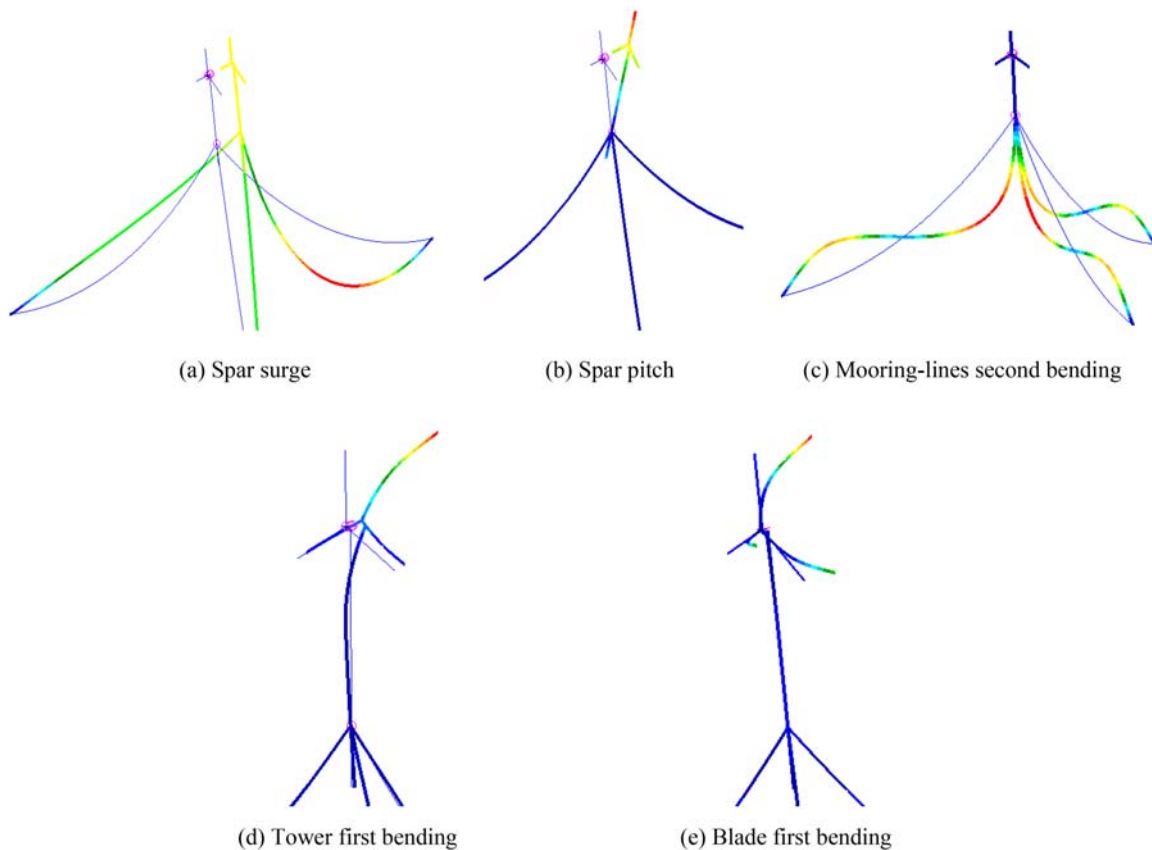

(a) Spar surge   (b) Spar pitch   (c) Mooring-lines second bending

(d) Tower first bending   (e) Blade first bending

Figure 6. Selected global modes of the integrated wind turbine (This figure is available in colour online.).

**Table 5.** The wave parameters of the load cases

Load Case	Average wind speed /m·s⁻¹	Wave Period/ s	Significant Wave Height/ m
Case 1	0	10	3
Case 2	11.4	10	3

catenary tension may significantly influence the structural strength and fatigue life. It is particularly noteworthy that slack-taut phenomenon, which may cause snap tension of the catenary, occurs if the catenary dynamics is considered. In Figure 7(c), at 10s period and 6 m amplitude of surge motion, there is an abrupt drop of the tension down to a minimum value, i.e. close to zero. And the top tension amplitude is about 3 times of the quasi-static one due to the catenary dynamics. The maximum top tension and tension gap at different amplitudes/frequencies of the top-end are given in Figure 8. It shows that the values of the maximum top tension (and the tension gap) get larger, e.g. up to 3.5 times of the static value particularly for the case of snap, with the increase of the amplitude and/or frequency of the top end motion.

3.1.2 The non-linear restoring stiffness and its hysteretic character

As presented above, the mooring-line dynamics could introduce an increase of top tension and tension amplitude difference. In fact, because of the involvement of dynamic behaviours, i.e. the inertial and damping effects, the restoring
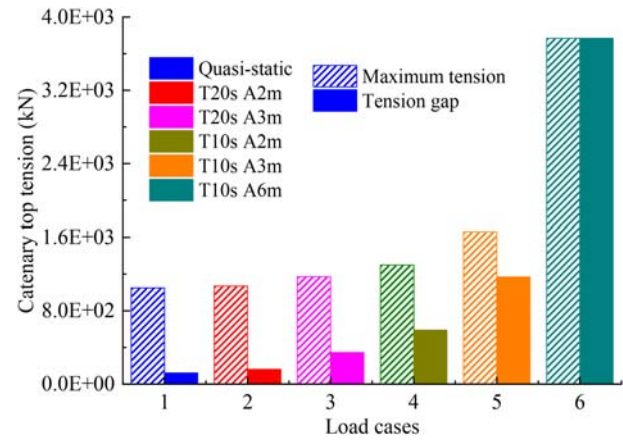
Figure 8. Top tension responses of the catenary mooring-line under different conditions (This figure is available in colour online.).

stiffness may also change. Thus, the restoring stiffness will be examined here, which is calculated under different top spar amplitudes, i.e. A varies from 3 to 7 m, along with different periods, i.e. T = 10, 20 and 40s. The selected results are presented in Figure 9.

Figure 9(a) shows the restoring stiffness curve of the whole mooring-lines system (involving lines 1, 2 and 3), at 20s period and 3.5 m amplitude, and also the static curve as a comparison. Interestingly, it is noted [in Figure 9(a,c)] that due to the damping effects coming from the structural bodies

(a) 20s period and 2m amplitude

(b) 10s period and 3m amplitude

(c) Time history of the top tension
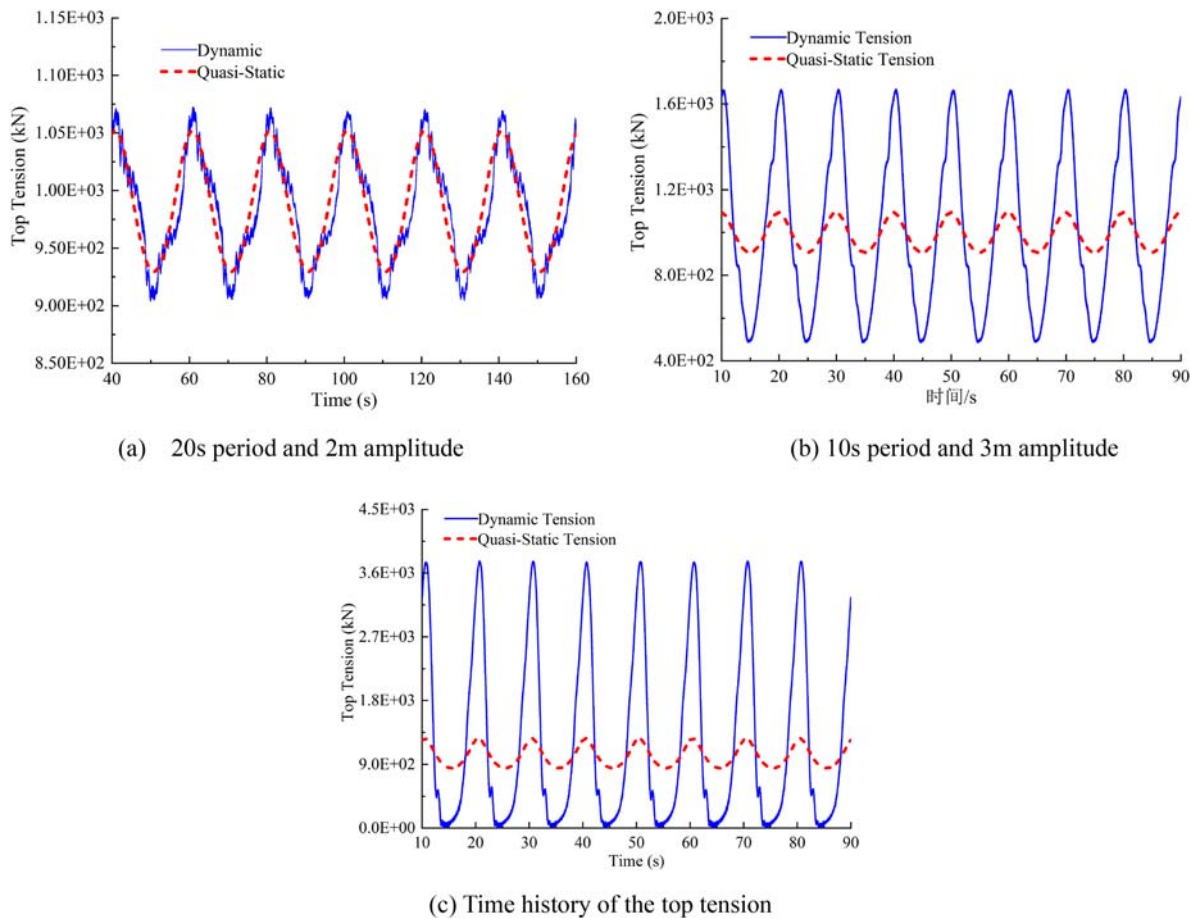
Figure 7. Time history of catenary top tension at different amplitudes and periods of spar surge (This figure is available in colour online.).
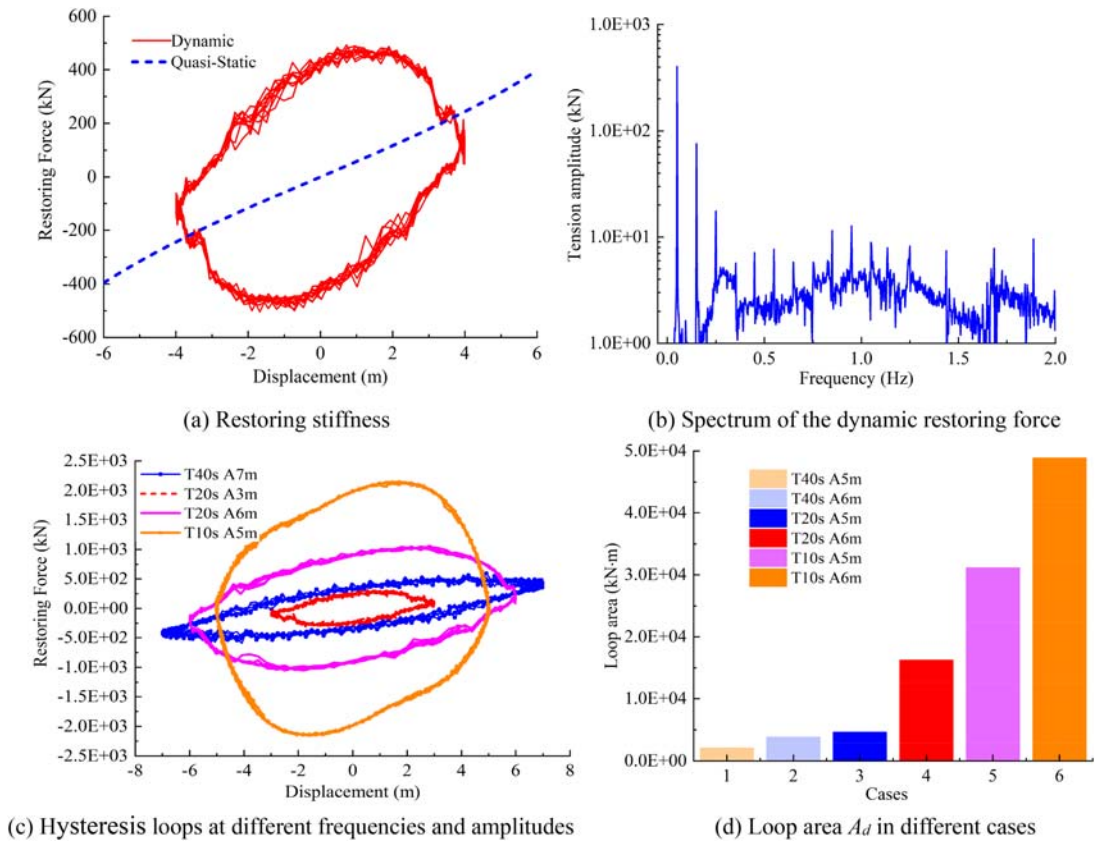
(a) Restoring stiffness

(b) Spectrum of the dynamic restoring force

(c) Hysteresis loops at different frequencies and amplitudes

(d) Loop area A_d in different cases

Figure 9. Restoring characteristics of the whole mooring-line system (This figure is available in colour online.).

(a) Time history of the spar surge

(b) Spectrum of spar surge

(c) Phase diagram of the spar surge
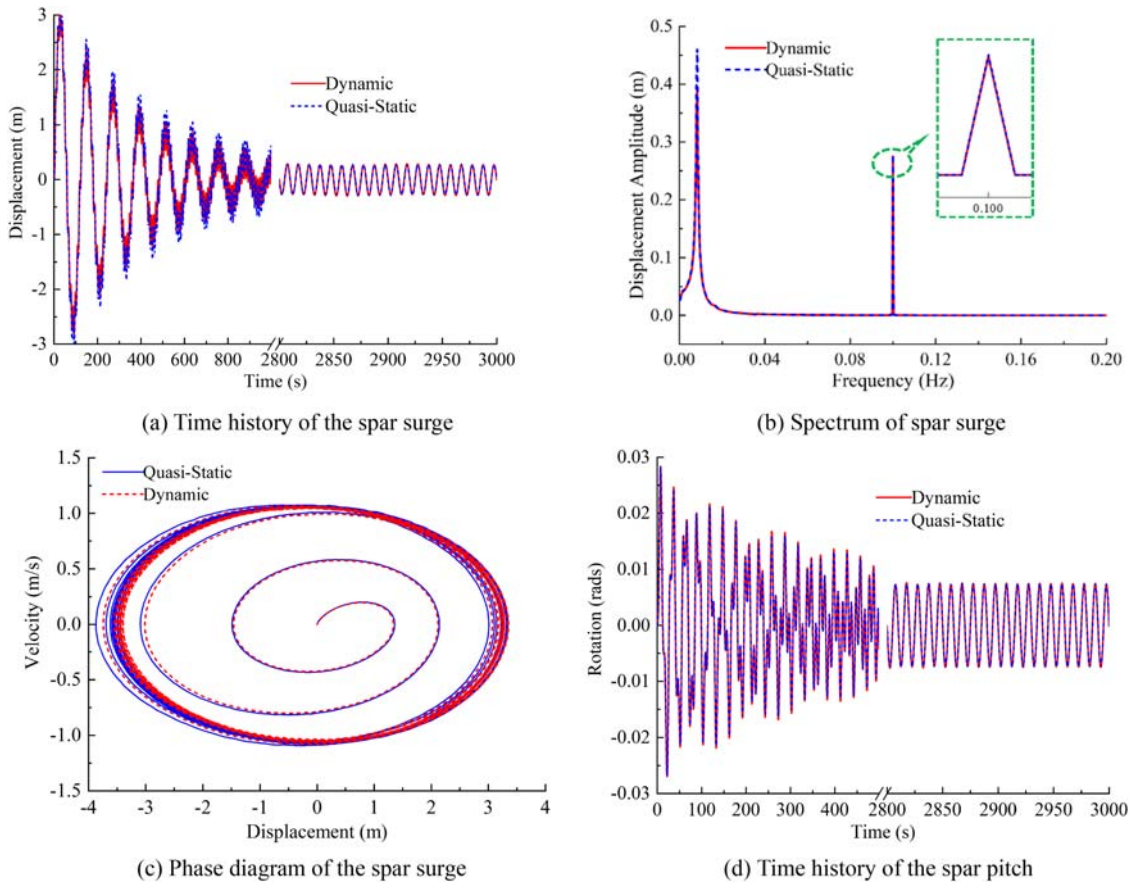
(d) Time history of the spar pitch

Figure 10. Surge and pitch response of the spar under regular wave (This figure is available in colour online.).
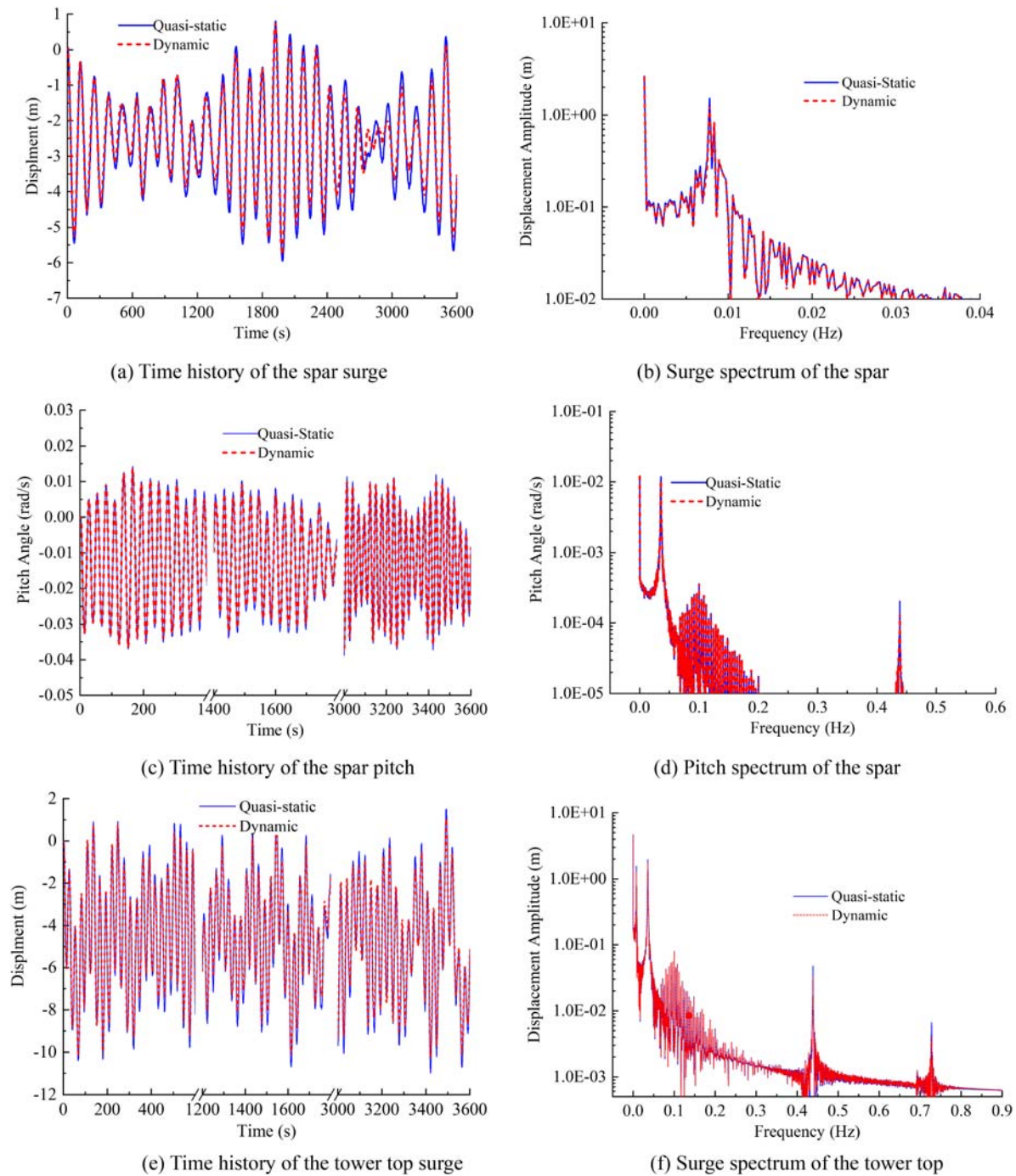
Figure 11. Displacement response of the wind turbine structures (This figure is available in colour online.).

and the fluid dynamics of the mooring-line, the restoring stiffness curve shapes approximately as an ellipse loop, called hysteresis loop. And, we can see that the restoring force depends on not only the spar displacement but also the spar velocity, or it does not get its maximum value at the maximum displacement but at a smaller displacement that provides a smaller dynamic stiffness, this is quite different from the static case. The spectrum plot, shown in Figure 9 (b), indicates that the peak values at frequencies of odd times of the excitation frequency are much larger than others. And, the loop area of the stiffness curve (or the energy consumption during a period) gets larger as the amplitude (and/ or the frequency) increases. In other words, the hysteresis

effect of the dynamic stiffness gets more obvious as the amplitude and/or frequency increase, as shown in Figure 9(c,d).

Given the profound damping effect coming from the dynamics of the mooring-line, we may say the dynamic response of the wind turbine will get smaller under the consideration of mooring-line dynamic behaviour, which will be presented and discussed in the following, i.e. in Section 3.2 and 3.3.

3.2. Dynamic response of the wind turbine under regular waves

Here the regular excitation frequencies are considered: the wave frequency is 0.1 Hz. To evaluate the influence of
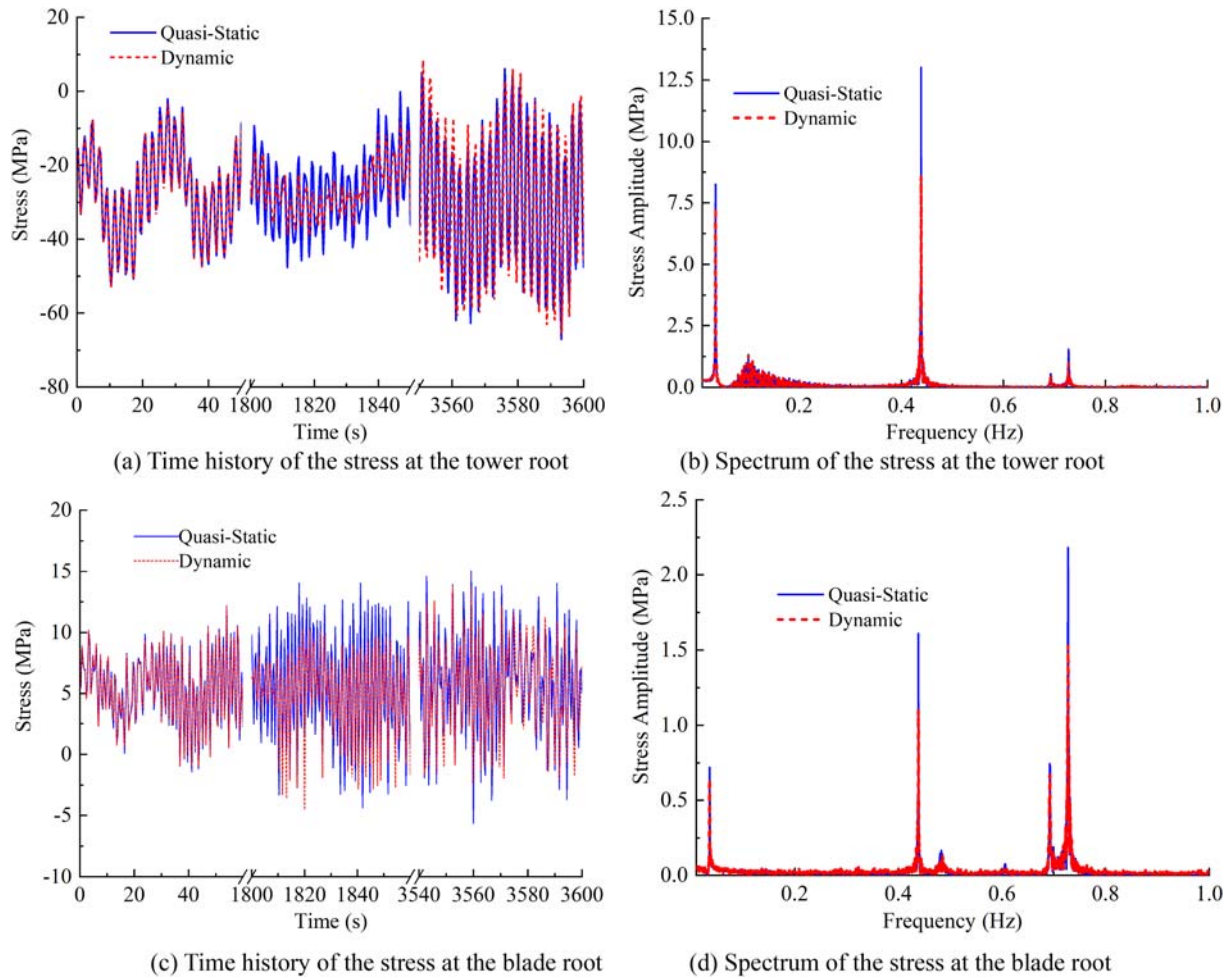
Figure 12. Structural stresses of the wind turbine (This figure is available in colour online.).

mooring-line dynamics on wind turbine response, the response under quasi-static restoring force is also calculated as a comparison.

The surge responses are compared in Figure 10(a,b). Slight difference is seen in Figure 10(a), except that the maximum surge displacement during the transient phase is about 11.4% smaller than the static. It means that the catenary dynamics has just a little influence on the global response. It is also noted that larger displacement happens during the transient phase and it gets much smaller during the steady phase. However, if considering the phase diagram shown in Figure 10(c), it can be seen that the motion amplitudes and motion trajectories of the spar are somewhat different from the quasi-static. As for the pitch motion shown in Figure 10(d), the displacement is almost the same with the quasi-static values, in both transient and steady phases. This is principally due to the spar stability property. In other words, the mooring system performs to provide the restoring stiffness to only the translational motion (surge, sway and heave), to a spar type of floating body. And the mooring system has little restoring control on its rotational motions such as roll and pitch, because the restoring force to control pitch or roll motions is mainly provided by hydrostatic buoyancy and spar structural gravity.

We may say that at the regular wave frequency excitation, the impact of mooring-line dynamics on the surge

displacement is not obvious. The influence of the mooring-line dynamics on the dynamic response of the wind turbine structures will be discussed in the later sections in detail.

3.3. Dynamic responses under random wind and wave loads

The cases of irregular waves are listed in Table 5, and the JONSWAP wave spectrum is used to get the time history of the wave velocity, and the wind velocity is calculated according to the Kaimal spectrum. Then the dynamic response of the integrated wind turbine is examined during 3600s time duration, while the phases of the wind and wave are considered as the same and the incident wave direction is along with the x axis (or the same with the surge direction of the floating spar).

The displacements and their spectrum, of the floating spar and the tower top, are presented in Figure 11. We found that the hysteretic character of mooring system restoring performance may lead to a decrease in the structural response, or the displacement peaks, for cases of dynamic and hysteresis behaviours being involved, are slightly smaller than the quasi-static ones. Besides the large value at 0 Hz, which is principally caused by the average wind velocity, the displacement is mainly dominated by the rigid body motion, i.e. the surge
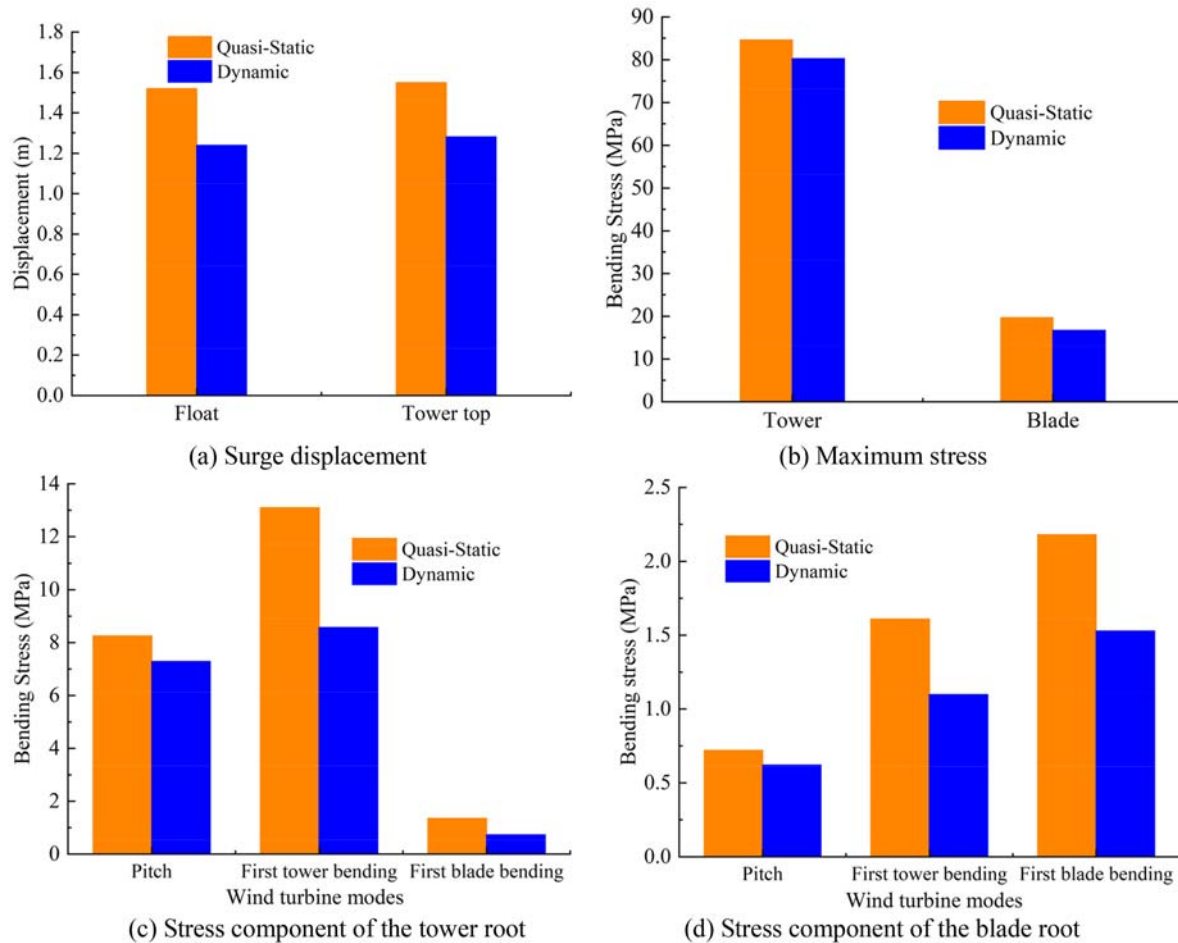
Figure 13. The structural responses under conditions of quasi-static and dynamic restoring forces (This figure is available in colour online.).

and pitch at 0.0083 and 0.0357 Hz frequency, respectively, while it involves some higher frequency component of elastic bending modes, e.g. 0.43 Hz/0.72 Hz of tower/blade first bending.

The structural stress and its spectrum, of the tower root and the blade root, are presented in Figure 12. It shows an obvious difference between the dynamic and the quasi-static ones, particularly at higher frequency. And, differently from the case of displacement response, the structural stress is mainly dominated by higher elastic frequency rather than the lower rigid body frequency, e.g. the higher values at 0.43 and 0.72 Hz of respectively the tower and blade bending frequencies. In addition, there are some additional peaks in the spectrum plot, see Figure 12(b,d), because the modes of the integrated wind turbine present some additional modes of the flexible bodies, e.g. those of the tower, blade and the mooring system. Or, our integrated FEM model can give the higher-order response of the wind turbine system under wind and wave loads, which is crucial to the fatigue life of the structure.

More specifically, the comparisons of the dynamic and quasi-static cases are presented in Figure 13. Generally speaking, under consideration of the dynamic behaviours and hysteretic characters of the mooring-lines, the value of spar displacement at surge frequency is 18.4%, i.e. 1.24 m compared to 1.52 m, smaller than the quasi-static one; and values of the

stress components are up to 32.7% smaller, i.e. 7.99 MPa compared to 11.77 MPa, than the quasi-static ones.

4 Conclusions

The structural dynamic responses of a large-sized floating wind turbine, undergoing wind and wave loads, are examined by the coupled FEM approach, and the flexible components, such as blades, tower, and mooring-lines, are included in the integrated system. To consider the catenary dynamics, the 3D flexible catenary model is combined with the modified FEM model. The catenary dynamics of the mooring-lines and its restoring performance are presented. And the impacts of mooring-line dynamics on the response of the integrated system under environmental loads are presented based on our numerical simulations. It is found that, owing to the fluid and structural damping, the dynamic stiffness presents a hysteresis loop, and the hysteretic behaviour becomes more obvious with the increase of frequency and amplitude. Our numerical results show:

(1). The maximum top tension of the catenary becomes larger due to the mooring-line dynamics. The top tension significantly increases with the increase of the spar motion, and particularly, the snap tension is 3 times larger than the quasi-static value.

(2). The restoring stiffness of the mooring-line presents a hysteresis loop due to its dynamics, and the loop area gets larger with the increase of body frequency/amplitude.

(3). Our coupled FEM model is able to give the higher-order response of the integrated wind turbine system under wind and wave loads, which is crucial to the fatigue life of the structure.

(4). The structural response gets smaller principally because of the hysteresis effect coming from the mooring-line dynamics. For example, the spar displacement at surge frequency is 18.4% smaller; the tower root stress at bending frequency is 32.7% smaller than the quasi-static value.

The dynamic response analysis of large-sized floating wind turbine under actions of wind and ocean wave/current is still a challenging issue. We hope that the presented FEM model can be further used as one of the useful approaches to analyse dynamic response and coupling mechanism between flexible components of wind turbines and other similar offshore structures.

Disclosure statement

Funding

ORCID

Weimin Chen ⓘ http://orcid.org/0000-0002-9060-9543

References

Azcona J, Palacio D, Munduate X, González. L, TA Nygaard. 2017. Impact of mooring lines dynamics on the fatigue and ultimate loads of three offshore floating wind turbines computed with IEC 61400-3 guideline. Wind Energy. 20:797–813.

Barooni AA, Ashuri T. 2018. An open-source comprehensive numerical model for dynamic response and loads analysis of floating offshore wind turbines. Energy. 154:442–454.

Barrera C, Guanche R, Losada IJ. 2019. Experimental modelling of mooring systems for floating marine energy concepts. Mar Struct. 63:153–180.

Browning JR, Jonkman J, Robertson A, et al. 2012. Calibration and validation of the FAST dynamic simulation tool for a spar-type floating offshore wind turbine. Proceedings of 2012 Science of Making Torque from Wind Conference.

Chen X, Zhang J, Ma W. 2001. On dynamic coupling effects between a spar and its mooring lines. Ocean Eng. 28(7):863–887.

Cheng ZS, Madsen HA, Chai W, et al. 2017. A comparison of extreme structural responses and fatigue damage of semi-submersible type floating horizontal and vertical axis wind turbines. Renew Energy. 108:207–219.

Christiansen S, Bak T, Knudsen T. 2013. Damping wind and wave loads on a floating wind turbine. Energies. 6(8):4097–4116.

Fazeres-Ferradosa T, Rosa-Santos P, Taveira-Pinto F, et al. 2020. Preface: advanced research on offshore structures and foundation design: part 2 [J]. Marit Eng. 173(4):96–99.

Giusti A, Stabile G, Marino E, et al. 2017. Coupling effects on the dynamic response of moored floating platforms for offshore wind energy plants. Procedia Eng. 199:3194–3199.

Guo S, Li Y, Li M, et al. 2017. Dynamic response of floating wind turbine under consideration of dynamic behavior of catenary mooring-lines. ASME 2017, International Conference on Ocean. 2017: V010T09A074.

Hall M, Buckham B, Crawford C. 2015b. Evaluating the importance of mooring line model fidelity in floating offshore wind turbine simulations. Wind Energy. 17(12):1835–1853.

Hall M, Goupee A. 2015a. Validation of a lumped-mass mooring line model with DeepC wind semisubmersible model test data. Ocean Eng. 104:590–603.

Hansen MOL. 2013. Aerodynamics of wind turbines. London: Taylor and Francis.

Jeon SH, Cho YU, Seo MW, et al. 2013. Dynamic response of floating substructure of spar-type offshore wind turbine with catenary mooring cables. Ocean Eng. 72:356–364.

Jonkman JM. 2007. Dynamics modeling and loads analysis of an offshore floating wind turbine. National Renewable Energy Laboratory, Golden, CO.

Jonkman JM. 2010. Definition of the floating system for phase IV of OC3. Golden, CO: National Renewable Energy Laboratory.

Jonkman JM, Buhl MLJr. 2007. Loads analysis of a floating offshore wind turbine using fully coupled simulation. Wind Power Conference and Exhibition; Los Angeles, CA.

Jonkman JM, Butterfield S, Musial W, et al. 2009. Definition of a 5-MW reference wind turbine for offshore system development. National Renewable Energy Laboratory, Golden, CO.

Kallesoe BS, Paulsen US, Kohler A, et al. 2011. Aero-hydro-elastic response of a floating platform supporting several wind turbines.49th AIAA Aerospace Sciences Meeting. Orlando, Florida.

Karimirad M. 2013. Modeling aspects of a floating wind turbine for coupled wave-wind-induced dynamic analyses. Renew Energy. 53:299–305.

Karimirad M, Moan T. 2012. Wave-and wind-induced dynamic response of a spar-type offshore wind turbine. J Waterw Port Coast Ocean Eng. 138(1):9–20.

Kim BW, Sung HG, Kim JH, et al. 2013. Comparison of linear spring and nonlinear FEM methods in dynamic coupled analysis of floating structure and mooring system. J Fluids Struct. 42:205–227.

Li YL, Guo SX, Li M, et al. 2018. Dynamic response analysis on the interaction between flexible bodies of large-sized wind turbine under random wind loads. Proceedings of the ASME 38th International Conference on Ocean, Offshore and Arctic Engineering. Madrid, Spain, June 17–22, 2018.

Masciola M, Robertson A, Jonkman JM, et al. 2013. Assessment of the importance of mooring dynamics on the global response of the DeepC-wind floating semisubmersible offshore wind turbine. In: Proceedings of the Twenty-Third(2013) International offshore and polar Engineering conference; Anchorage, Alaska, USA.

Matha D, Bischoff O, Fechter U, et al. 2011. Non-linear multi-body mooring system model for floating offshore wind turbines. EWEA offshore 2011. Amsterdam, Netherlands. 29 November-1 December, 2011.

Matha D, Fischer T, Kuhn M, et al. 2010. Model development and loads analysis of a wind turbine on a floating offshore tension leg platform. European Offshore Wind Conference and Exhibition, Stockholm, Sweden.

Palm J, Paredes GM, Eskilsson C, et al. 2013. Simulation of mooring cable dynamics using a discontinuous Galerkin method. In: Proceedings of V International Conference on Computational Methods in Marine Engineering; Hamburg, Germany.

Park K-P, Cha J-H, Ku N. 2016. The flexible multibody dynamics of a floating offshore wind turbine in marine operations. Ships Offsh Struct. 1–12. DOI: 10.1080/17445302.2016.1187373.

Rajeswari K, Nallayarasu S. 2020. Hydrodynamic response of three- and four-column semi-submersibles supporting a wind turbine in regular and random waves. Ships Offsh Struct. 1–11. DOI: 10.1080/17445302.2020.1806681.

Robertson AN, Jonkman JM. 2011. Loads analysis of several offshore floating wind turbine concepts. International Society of Offshore and Polar Engineers Conference, Maui, Hawaii. June 19-24.

Sagrilo LVS, Siqueira MQ, Ellwanger GB, et al. 2002. A coupled approach for dynamic analysis of CALM systems. Appl Ocean Res. 24(1):47–58.

Sethuraman L, Venugopal V. 2013. Hydrodynamic response of a stepped-spar floating wind turbine: numerical modelling and tank testing. Renew Energy. 52:160–174.

Shin H, Pham TD, Jung KJ, et al. 2013. Model test of new floating offshore wind turbine platforms. Int J Nav Archit Ocean Eng. 5(2):199–209.

Stewart G. 2012. Calibration and validation of a FAST floating wind turbine model of the DeepC wind Scaled Tension-Leg Platform: Preprint. Office of Scientific & Technical Information Technical Reports.

Tanaka K, Sato I, Utsunomiya T, et al. 2020. Validation of dynamic response of a 2-MW hybrid-spar floating wind turbine during typhoon using full-scale field data. Ocean Eng. 218:108262.

Wang K, Ji C, Xue H, et al. 2016. Frequency domain approach for the coupled analysis of floating wind turbine system. Ships Offsh Struct. 1–8. DOI: 10.1080/17445302.2016.1241365.

Waris MB, Ishihara T. 2012. Dynamic response analysis of floating offshore wind turbine with different types of heave plates and mooring systems by using a fully nonlinear model. Coupled Syst Mech. 1 (3):247–268.